RESEARCH ARTICLE

Effect of Water Injection Rate on the Distribution of Water-driven Oil in the Tankou Oilfield

Yuan Yang[1] **and Ye Yang**[2,*]

[1] Exploration and Development Research Institute, Jianghan Oilfield Company, Sinopec, Wuhan 430223, China
[2] Drilling Company No.1 of Sinopec Jianghan Petroleum Engineering Co., Ltd., Qianjiang, 433123, China

Abstract

Supplementing formation energy through water injection is the main way to develop old oil fields. However, formation non-homogeneity leads to the uncertainty of waterline advancement, which generates residual oil. In order to study the effect of water injection rate on the distribution of water-driven oil, we carried out water injection simulation experiments using the Tankou oilfield as an example. The oil saturation contour maps of several time points in the water-driven oil process were plotted by determining the trend of resistance value changes. We studied the drive path during the water-driven oil process, determined the location of residual oil distribution in the plane and longitudinal direction and analysed the reasons for residual oil generation. The study concludes that the optimal upper limit of the water injection rate in this area is 15 ml/min, which is converted to 24 m^3/day in the case of low injection and high recovery. In the case of high injection and low recovery, the daily water injection rate is 20 m^3 to verify the effect.

Keywords: residual oil, injection rate, waterline advancement, resistance value, tankou oilfield.

1 Introduction

China's onshore oilfields have successively entered the late stage of development, which requires water-driven oil development, and this process makes the oilfields enter the period of high water content, so the recovery of residual oil is very important [1, 2]. How to adjust the layer position and control the injection and recovery parameters under the premise of existing well network deployment to achieve the uniform advancement of water-driven profile is an urgent engineering problem. Among them, the effect of water injection rate on water-driven residual oil is very important. Higher water injection rate can increase the driving efficiency of residual oil and thus improve the recovery rate [3].

Currently, the research on the injection rate on water-driven residual oil mainly focuses on the mechanism, physical experiments and oilfield applications. Chen et al. [4] used nuclear magnetic resonance (NMR) analysis experiments in combination with the classical capillary number theory to carry out the effect of injection rate on water-driven in unconventional oil and gas reservoirs. It was found that increasing the injection rate of tight

Submitted: 16 April 2026
Accepted: 20 May 2026
Published: 26 May 2026

Vol. 2, **No.** 2, 2026.
10.62762/JGEE.2026.867883

***Corresponding author:**
✉ Ye Yang
kalimoto1977@yeah.net

Citation
Yang, Yuan, & Yang, Ye (2026). Effect of Water Injection Rate on the Distribution of Water-driven Oil in the Tankou Oilfield. *Journal of Geo-Energy and Environment*, 2(2), 163–177.

oil cores can significantly increase the recovery rate, and this significant increase is mainly attributed to mesopores and micropores. Tan et al. [5] carried out a study on the resonance-enhanced pulse water injection to improve the recovery rate through the construction of a microscopic model. When the pulse frequency is matched with the intrinsic frequency of the microscopic model, resonance occurs in the process of pulse-driven two-phase flow, which results in the amplitude of the oscillation increasing and the mobility of crude oil being enhanced. Liu et al. [6] investigated the effect of wettability on the microdistribution of oil and water and production performance in tight reservoirs by NMR measurements and rate-controlled piezomercury tests. It was derived that, as wettability changed from strong water wetting to weak oil wetting, oil was adsorbed on the pore and throat surfaces and migrated from the centres of larger pores to smaller pores and/or throats. Due to the narrowing of the two-phase flow zone, the water saturation at the isotonic point decreases, which affects the oil seepage and leads to lower water injection recovery. Saadat et al. [7] carried out a visualisation study of the unmixed-phase fluids displacing residual oil in a porous medium by using a microfluidic model in combination with a flat-plate sandpack model to evaluate the intrusion patterns, displacement processes and improvement methods. Xu et al. [8] developed a three-dimensional homogeneous model to simulate SAGD scenarios with or without mitigation, resulting in the proposed use of gas/water replacement to mitigate the effects of depletion in order to reduce depletion impacts and improve the SAGD performance. Zhang et al. [9] carried out an experimental study of nitrogen foam driving through one-dimensional core tube experiments. The oil repulsion characteristics of nitrogen foam in oil and water reservoirs with thick layers of high porosity and high permeability were obtained, and the mechanism of water plugging in the regulating section was analysed. Shapoval et al. [10] evaluated the physicochemical interactions in the process of water injection into reservoirs through geochemical modeling and experiments, and explained the mechanism of the influence of capillary force at the pore scale. Wei et al. [11] carried out experimental studies on oil repulsion and surfactant-polymer repulsion by means of microscale oil repulsion experiments, and carried out experimental studies on water drive and surfactant-polymer drive for residual oil distribution and recovery using NMR technique. It was concluded that the limit of SP drive contribution to pore throat diameter was much lower than that of water drive.

However, most of the existing results have a single research method, mostly software simulation and phenomenon interpretation, lack of indoor experiments combined with on-site development of a comprehensive description, while there is no specific development programme recommended by the operating parameters of the preferred [12, 13]. Therefore, this paper takes the X well area of the Tankou oilfield as the research object, clarifies the seepage characteristics of different small layers and residual oil distribution characteristics of different types of fracture block reservoirs with the help of flat plate sand filling experiments; explores the influence of the water injection rate on the distribution of residual oil under the fixed injection and extraction methods, and establishes corresponding mathematical empirical models to depict the morphology of the water-driven oil flow line and study the replacement paths. Explore the residual oil distribution in the plane and longitudinal direction and analyse the reasons for residual oil generation.

2 Geological setting

Displacement efficiency, permeability adjustment, and oil-water separation all affect the water injection rate to different degrees [14]. Firstly, a higher water injection rate can push water into the formation more efficiently and reduce the chance of oil-water mixing, which in turn reduces the saturation of the remaining oil [15]. This will lead to higher replacement efficiency, i.e., more remaining oil is driven from the formation; secondly, higher water injection rate can effectively adjust the permeability distribution of the formation. When the water injection rate is higher, the water will penetrate more rapidly through the channels with higher permeability to more distant locations, thus slowing down the water flow rate in the higher permeability region and increasing the displacement effect on the low permeability region [16–18]; finally, the higher injection rate can increase the opportunity of the oil-water phase contact, and promote the separation of the oil and water [19]. When the water injection rate is low, the interfacial tension between oil and water is greater due to the longer mixing time between water and oil, resulting in difficulty in driving the oil out.

The Tankou oil field belongs to the typical complex fault block reservoir type in eastern China. The regional structure belongs to the Zhongtan Fracture

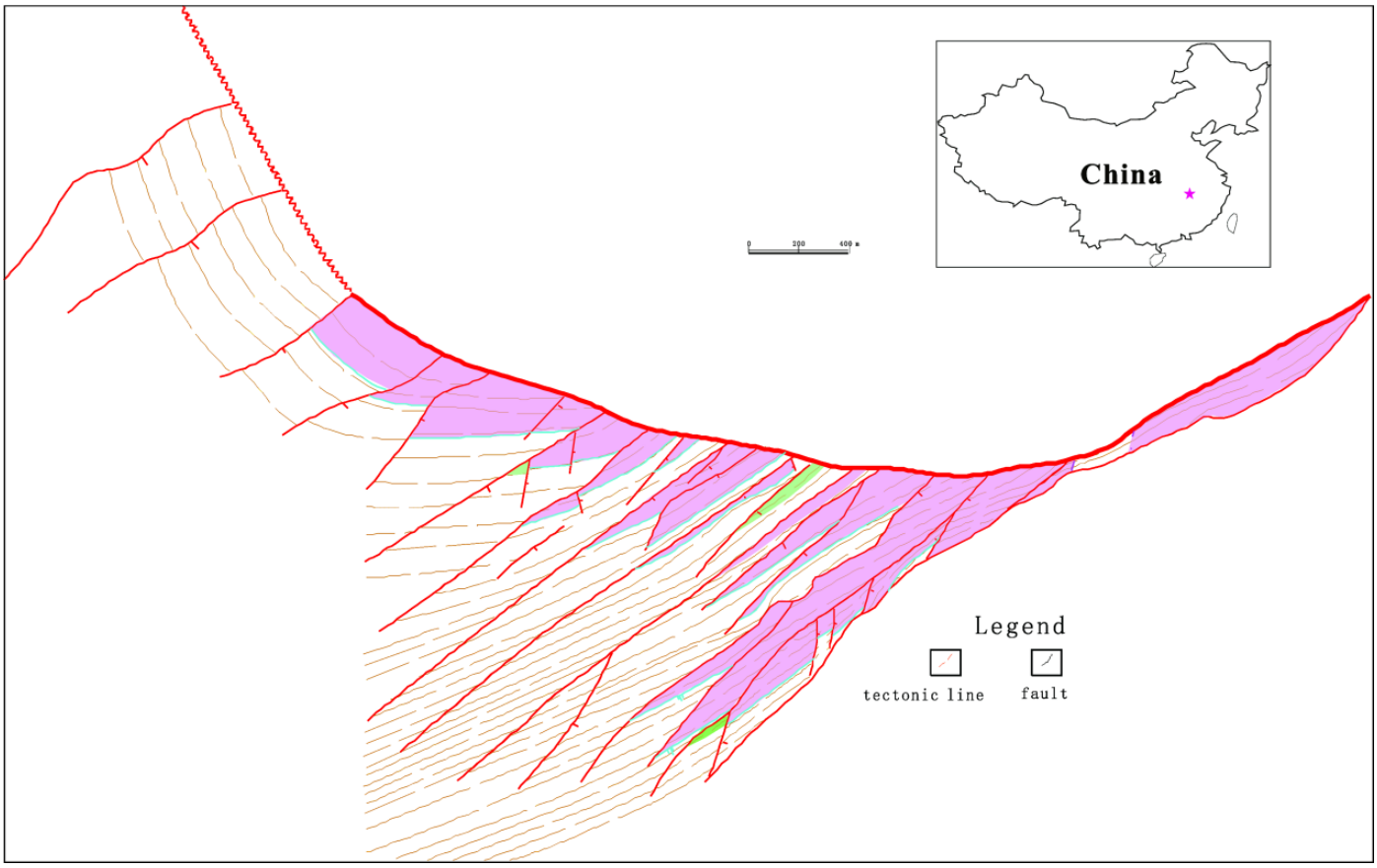

Figure 1. Tectonic map of the top surface of submerged 41 in the western slope zone of the Tankou Bulge.

Zone in the north of Qianjiang Depression in the Jianghan Basin (Figure 1). The X well area is located in the east of the Tankou oil field. There are many oil-bearing layers, mainly concentrated in the $Eq4^1$, $Eq4^1x$, $Eq4^0$, $Eq4^0x$, $Eq4^2$, $Eq4^3$ and other oil groups [25]. The oil layer buried depth is 660 m–2945 m, the dip angle of the strata is 45° 60°, the average porosity of reservoir is 23.8%, permeability 534.2×10^{-3} μm^2, surface crude oil density 0.863–0.920 g/cm^3, surface crude oil viscosity 21.2–63.8 mPa·s, original formation pressure 12.6–29.5 MPa, saturation pressure 0.70–2.2 MPa, pressure coefficient 1.12. It belongs to the medium pore and medium seepage and high steep structure extremely complex fault block reservoir [20–22]. Its main geological characteristics are as follows: low-order faults are extremely developed with small fault blocks; the thickness and permeability of oil-bearing pay zones vary greatly, resulting in strong interlayer heterogeneity; the oil-water relationship is complex and natural energy differs significantly. The area is generally developed with an inverted nine-spot well pattern [24]. The area is generally developed with an inverted nine-spot well pattern, which is commonly adopted in fault-block reservoirs in eastern China for its favorable sweep efficiency under complex geological conditions [23]. Well locations are not marked due to the confidentiality of geological data.

There are 51 oil wells and 15 water wells in X well area of Tankou oil field, with daily oil production of 109.7 t, average daily production of single well is 2.2 t, comprehensive water content is 49.4%, daily water injection is 244.5 m^3. Until now, the cumulative oil extraction is 66.8×10^4 t, the oil extraction speed of geological reserves is 0.89% (calculated according to the recalculated reserves), and the extraction speed is moderately low; the current injection/extraction ratio is 0.96, and cumulative water extraction is 44.23×10^4 m^3, cumulative water injection 52.83×10^4 m^3, and cumulative injection ratio is 0.42, and the formation deficit is serious, and the extraction degree of geological reserves is low (15.72%). The current calibrated recovery rate is 38.7%, which has a large potential for development and adjustment to increase production, but due to its geological structure, fluid properties, oil and water system complexity and specificity [26, 27]. Experimental assistance is needed to derive development and adjustment measures for the old oil area, optimise the current development parameters and achieve stable production.

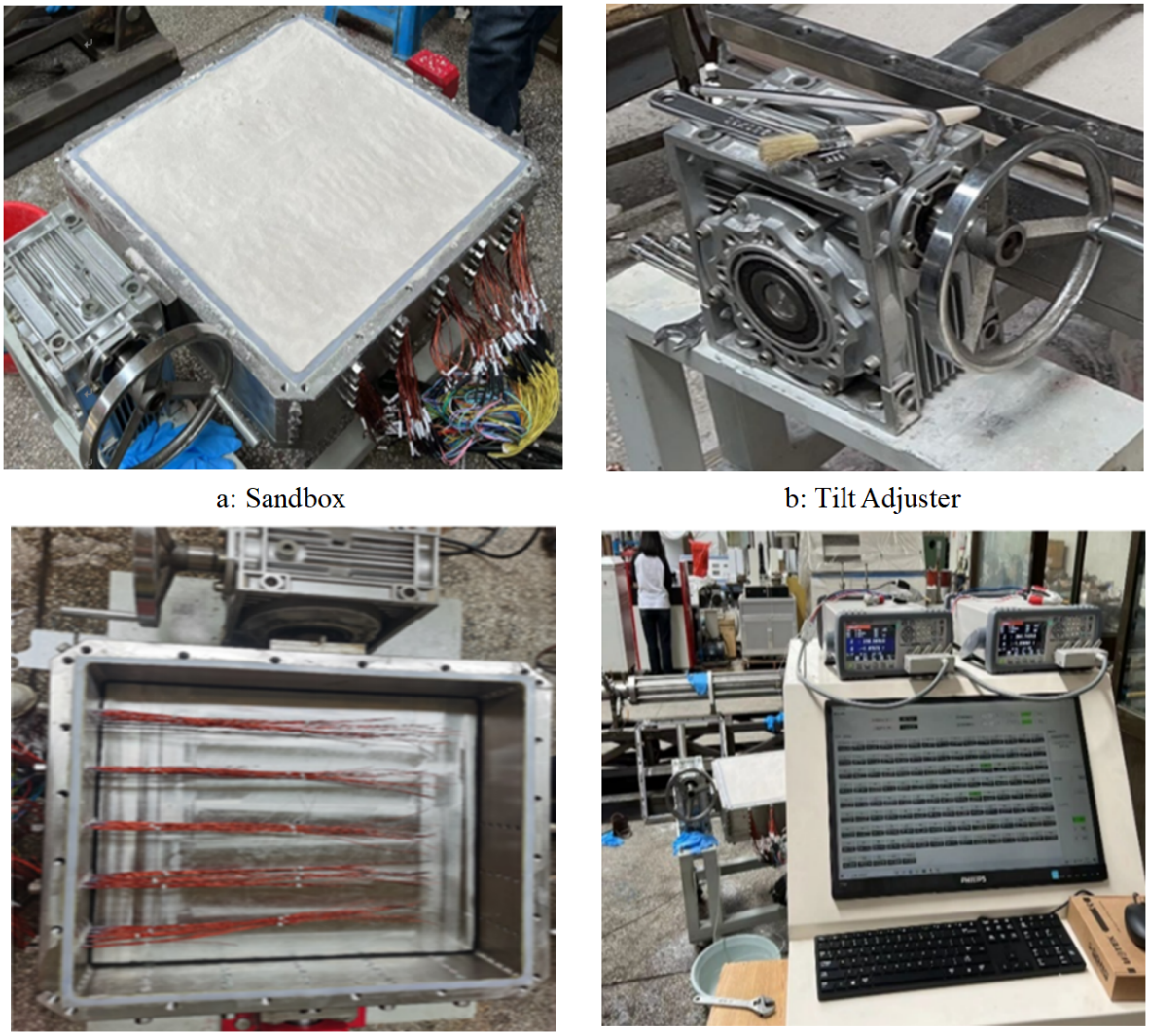

a: Sandbox b: Tilt Adjuster

c: Resistive d: Measurement terminals

Figure 2. Key experimental materials and equipment.

This study focuses on exploring the influence of water injection rate on the distribution of water-driven oil in the X-well area of the Tankou Oilfield. A three-dimensional physical model of water-driven oil was designed by ourselves, and the experimental study was carried out under a single influencing factor without discussing the model inclination angle, reservoir physical properties, and the coupling of injection and extraction.

3 Materials and methods

The size of this model is 500mm×500mm×100mm, divided into 5 layers on average, each layer has 25 resistance detection points distributed evenly in each plane, a total of 125 resistance detection points. The whole model is made of stainless steel, which can fully prevent the corrosion of the injected liquid on the sand box model, and the upper end of the model is made of plexiglass panel, which can observe the oil injection process and the water drive process, the fluid direction of the first layer on the surface, and record the observation phenomenon through the camera so as to correct the experimental scheme in time. The top view of the model is square, and the overall shape is rectangular, with 20 openings at the four corners to simulate the extraction wells and injection wells.

The experimental setting is one injection and one extraction. The oil saturation contour maps of several time points in the process of water-driven oil were plotted through the determination of the trend of resistance value changes. The driving path in the process of water-driven oil was studied to determine the distribution of residual oil in the plane and longitudinal direction and to analyse the reasons for the residual oil generation. Finally, the final recovery rate is estimated from the decline in oil saturation and

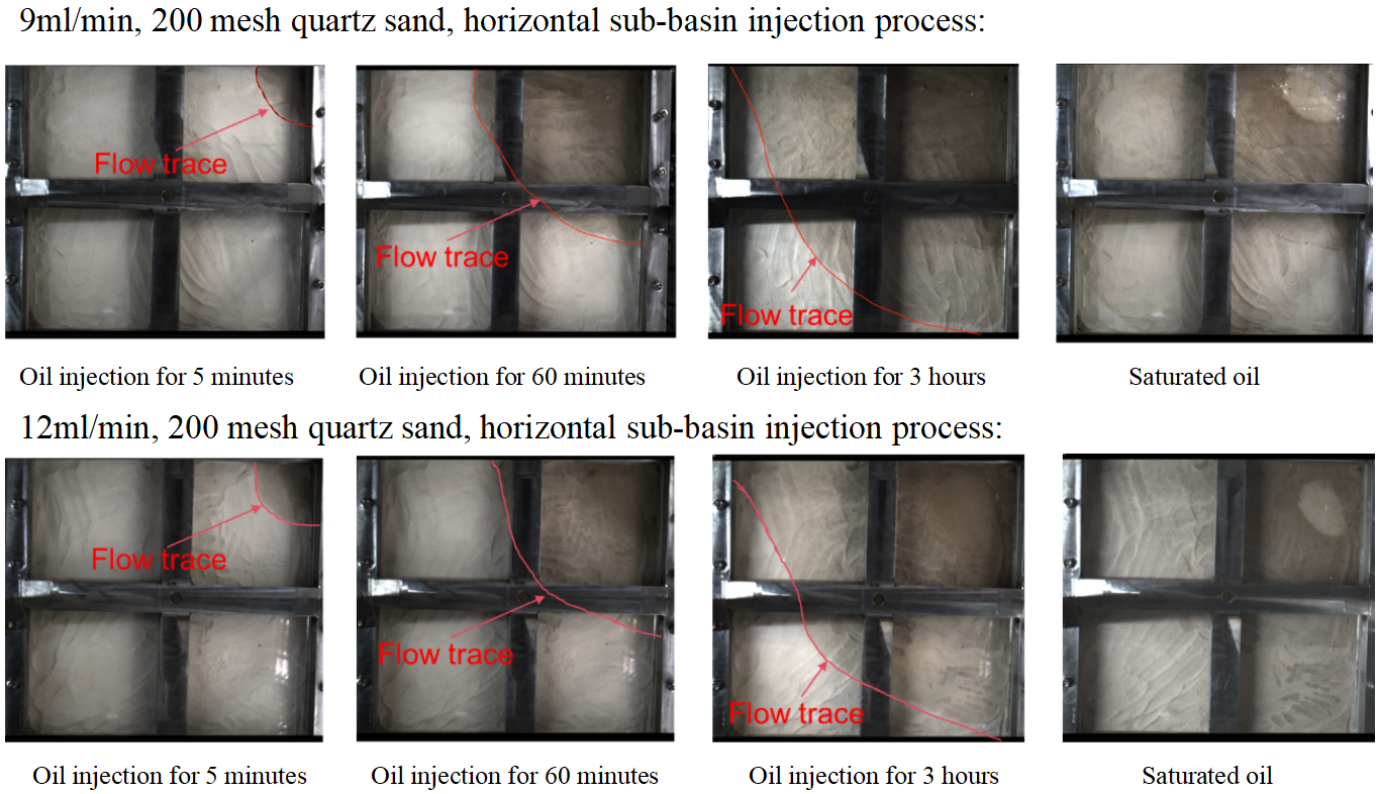

Figure 3. Flow trace diagram of water injection process.

compared with the actual recovery rate.

Materials and equipment: sand box, inclination adjuster, resistance sensors, measuring terminals (Figure 2).

The experimental steps are as follows:

1. Fill the sand box of 500 mm × 500 mm × 100 mm with 200 mesh quartz sand and add the cover to make sure the experimental device is sealed and the inclination is horizontal.
2. Inject 2.08 L of paraffin into the inside of the experimental setup at a constant speed and pressure of 5 ml/min.
3. Mix 40 g NaCl into 1 L of water and execute the expulsion at injection rates of 3 ml/min, 6 ml/min, 9 ml/min and 12 ml/min, respectively.
4. Record the flow traces of water and oil; record the resistance value data during water injection every 3 minutes, and draw the contour plot of resistance of remaining oil distribution. Measure and record the time of seeing oil, time of seeing water, time of pure water, oil production, water production, liquid production, and the rule of change of each production with time during the process of water driving oil.
5. Through the measurement terminal, obtain key parameters such as oil production rate, water production rate, liquid production rate, final extraction degree, and residual oil saturation by conversion.

4 Results

From oil injection to water injection, we used a camera to record the flow traces of experimental water and oil in real time, which facilitated the observation of residual oil movement as well as the location of residual oil, and the verification of the subsequent analyses (Figures 3 and 4).

As can be seen in Figures 3 and 4, with different injection rates, the water-driven oil flow trajectory is diagonal arc forward from the injection end to the oil end, and in the same time, the oil-driving speed and oil-sweeping area of the 12 ml/min injection rate is higher than that of the 9 ml/min injection rate, and the residual oil distribution of the high injection rate is more scattered compared with that of the low injection rate.

The resistivity data in the experiment is important to reduce the saturation of the remaining oil, we recorded the resistance value data several times every 3 minutes during the injection process, and processed

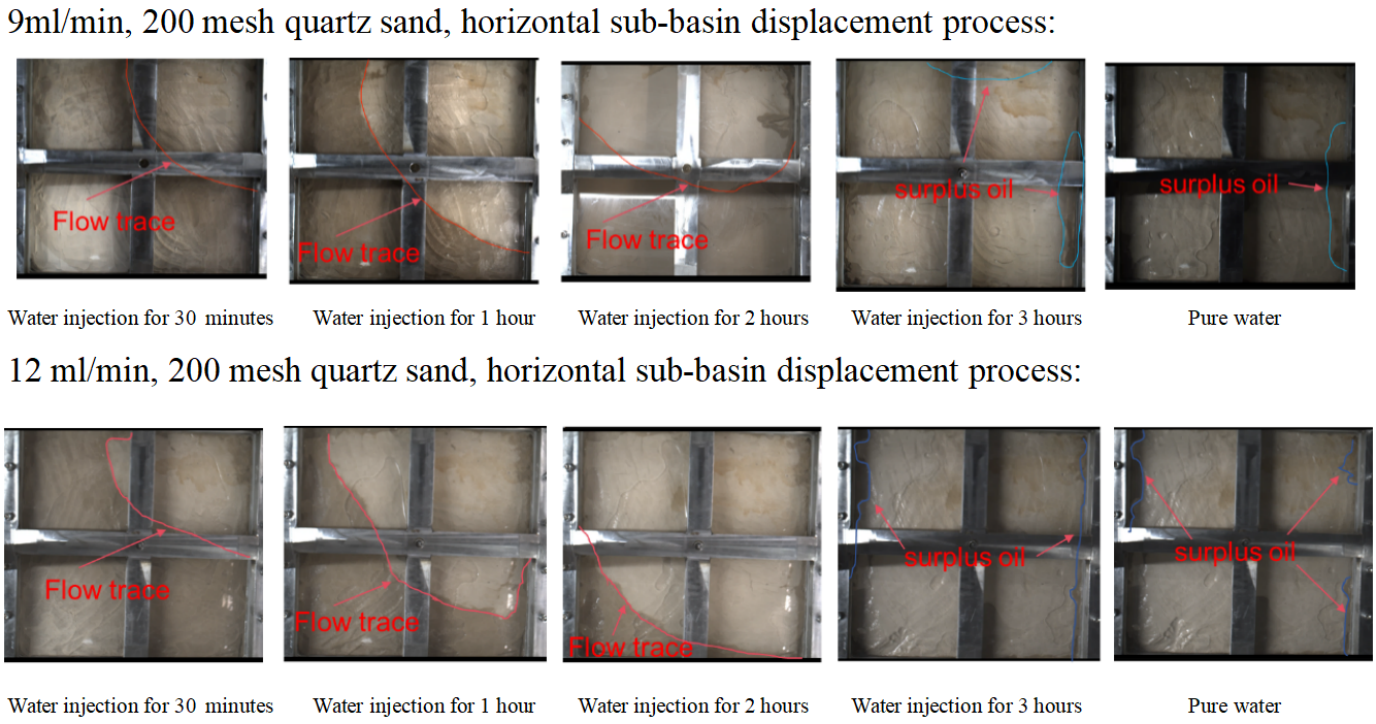

Figure 4. Flow trace diagram of the oil injection process.

and analysed the resistance value according to the theory that oil has higher resistivity than water, and used the surfer software to produce a contour plot of the resistance of the remaining oil distribution.

One injection and one production, 9ml/min, 200 mesh quartz sand, displacement process under horizontal formation:

It can be seen through Figure 5, blue represents water, red represents oil, the darker the colour indicates higher water content, with the increase of water injection time, the water line along the diagonal arc to the front of the replacement of oil, with the increase of the time of replacement, the remaining oil from the outlet to the left and right sides of the diagonal gradually move, and ultimately mainly in the perpendicular to the direction of the water line to advance the mainstream of the diagonal of the two sides of the distribution.

The effect of injection rate on the time to see oil and water. We carried out four groups of experiments as a control, the parameters in the horizontal inclination, 200 mesh quartz sand, one injection and one extraction, only change the injection rate, take the data of the time to see water and oil to make the time to see water and oil with the injection rate change curve (Figure 6). The figure shows that the larger the injection rate, the shorter the time to see oil and water. With the increase of water injection rate, the time of seeing water-100% water content is shorter. And the effect of water injection rate on the time to see oil is much smaller than the effect of the time to see water as well as the time to pure water. Especially, after 3 ml/min and 6 ml/min decline rate is far more, it can be seen that 3 ml/min water injection rate is completely insufficient to support the driving force required for water-driven oil experiments.

The effect of water injection rate on oil and water production rate. The significance of the rate of oil and water production to the experiment is crucial, which will directly affect the final crude oil output, so we chose to analyse the rate of oil, water and liquid production of these four groups of experiments, where the rate of oil production = the amount of oil produced in the water-oil mixture/time, the rate of water production = the amount of water produced in the water-oil mixture/time, and the liquid production is the sum of the two (Figure 7).

As can be seen in the Figure 7, the water and oil production rates increase exponentially with the increase of water injection rate within a certain range. However, the increase in oil production rate is not obvious, which may be due to the gradual decrease of crude oil within the model, and the water will be more easily flushed out after the formation of the dominant channel.

The effect of water injection rate on the final

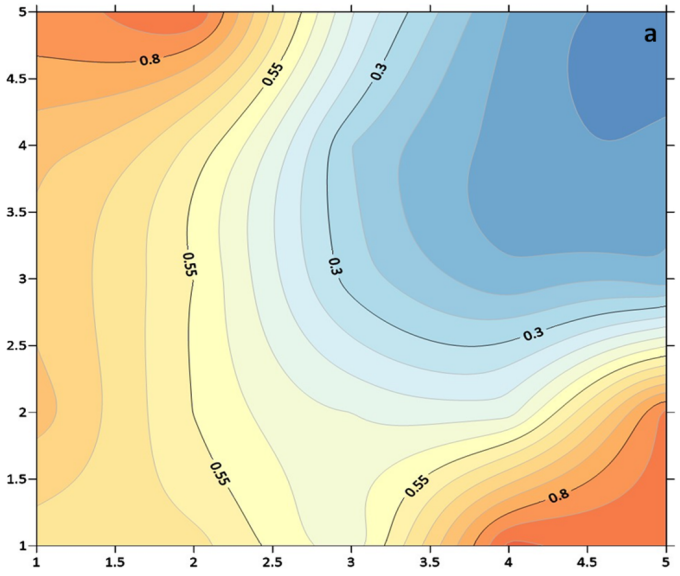

a. Resistivity contour plot（170min-Oil release）

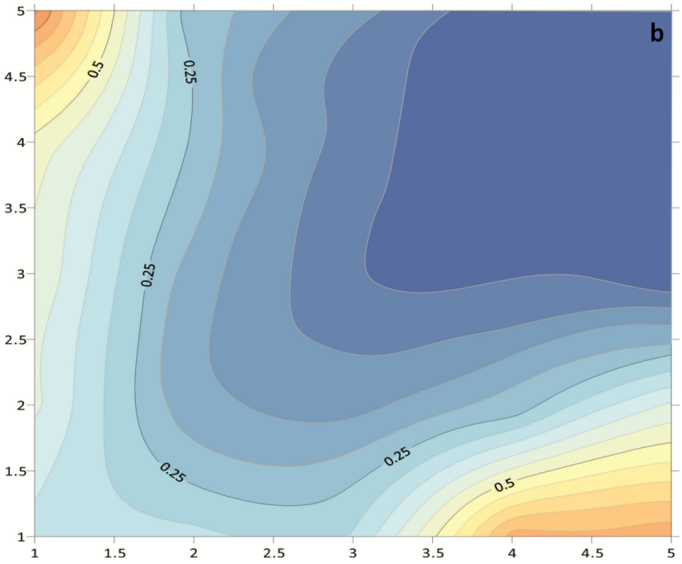

b. Resistivity contour plot（385min- during oil production）

Figure 5. Resistivity contour plots at different stages of water flooding.

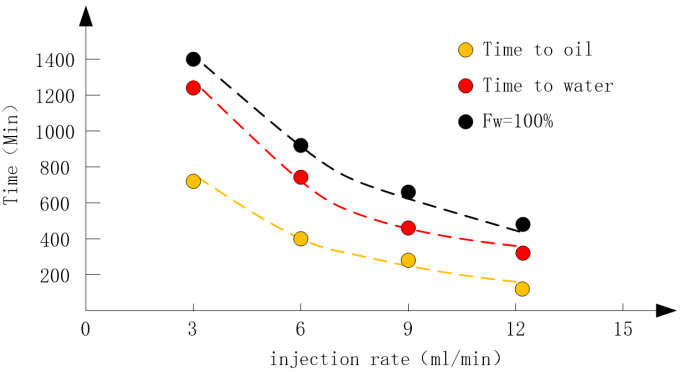

Figure 6. Variation curve of time to see water and oil with injection rate.

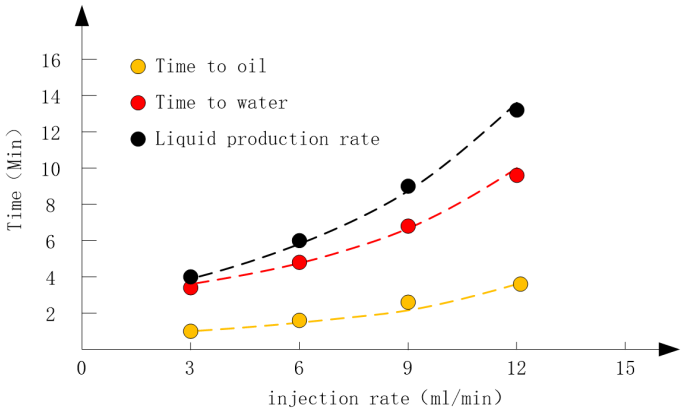

Figure 7. Curve of oil and water discharge rate variation with water injection rate.

recovery degree. Final recovery degree = final oil production/total oil in the model, and we made a linear fit to the final recovery degree based on the four sets of experiments of water injection rate (Figure 8).

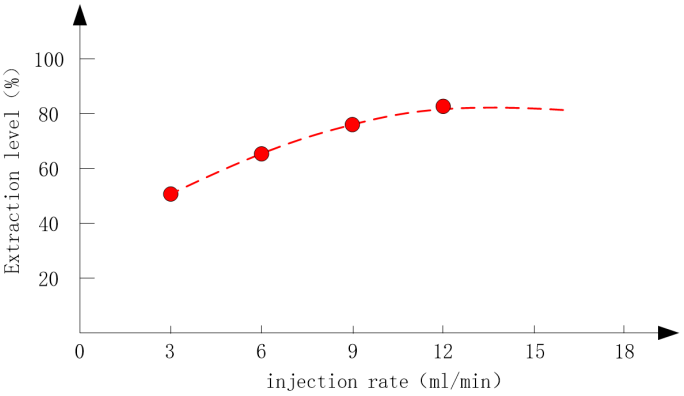

Figure 8. Curve of final degree of extraction versus water injection rate.

The graph shows that the final degree of extraction increases with increasing injection rate. A one-fold increase in the injection rate increases the ultimate extraction level by about 1/4. The ultimate extraction level increases binomially with increasing injection rate, and it is expected that the optimal injection rate is at 15 ml/min, the inflection point of the binomial, which is about 80%, and then the ultimate extraction level decreases as the injection rate increases.

Influence of water injection rate on final residual oil saturation. The final residual oil saturation refers to the ratio of the residual oil volume in the model to the total liquid volume in the model, and the analysis of the final residual oil saturation can intuitively understand the situation of the residual oil in the model, speculate the location of the residual oil, and guide how to improve the recovery rate. The final residual oil saturation diagram of the water injection rate experiment was

fitted (Figure 9).

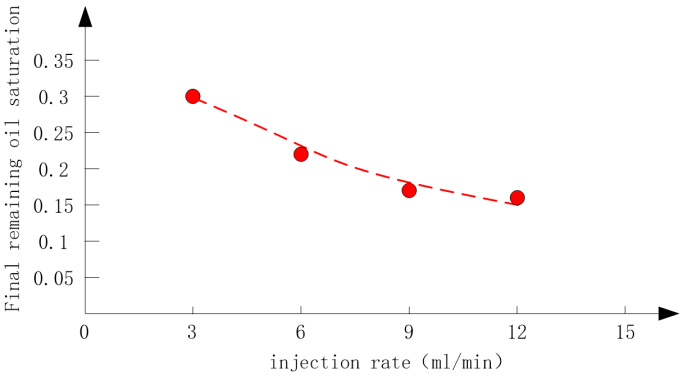

Figure 9. Variation curve of final residual oil saturation with injection rate.

It can be seen from the Figure 9 that the final residual oil saturation decreases with the increase of injection rate, and the two have a logarithmic relationship. The larger the injection rate is, the smaller the remaining oil is, and the better the extraction effect is.

For different injection rates, the variation of production with time provides a more intuitive understanding of oil production and water production rates at different moments. The following figure shows the oil production vs. time curves for the four groups of experiments at different injection rates. The slope of each curve represents the oil production rate at that moment.

The fitting functions of oil production with time under different water injection rates are as follows:

- Injection rate of 3 ml/min:

$$y = 1962.4\ln(x) - 4652.1, \quad R^2 = 0.9858$$

- Injection rate of 6 ml/min:

$$y = 1678.1\ln(x) - 2641.1, \quad R^2 = 0.964$$

- Injection rate of 9 ml/min:

$$y = 1775\ln(x) - 1949.2, \quad R^2 = 0.972$$

- Injection rate of 12 ml/min:

$$y = 1860.7\ln(x) - 1261.5, \quad R^2 = 0.9776$$

These results are shown in Figure 10.

The fitting functions of water production with time under different water injection rates are as follows:

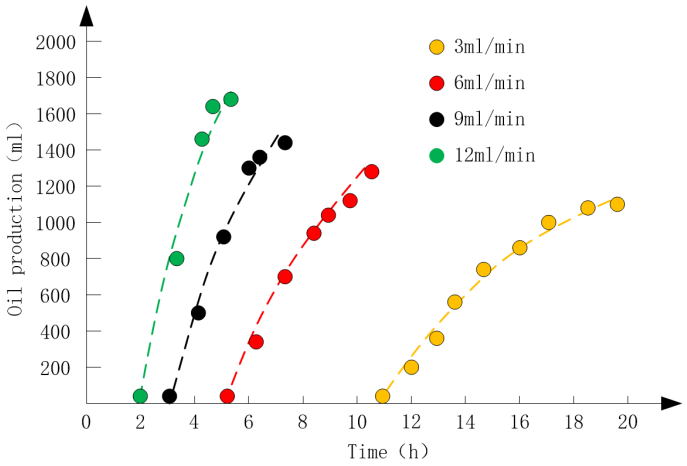

Figure 10. Law of change of oil production with time.

- Injection rate of 3 ml/min:

$$y = 129.29x - 2218.6, \quad R^2 = 0.9967$$

- Injection rate of 6 ml/min:

$$y = 285.5x - 2426.3, \quad R^2 = 0.9993$$

- Injection rate of 9 ml/min:

$$y = 536.32x - 3041.7, \quad R^2 = 0.9999$$

- Injection rate of 12 ml/min:

$$y = 980.84x - 3948.3, \quad R^2 = 0.9891$$

These results are shown in Figure 11.

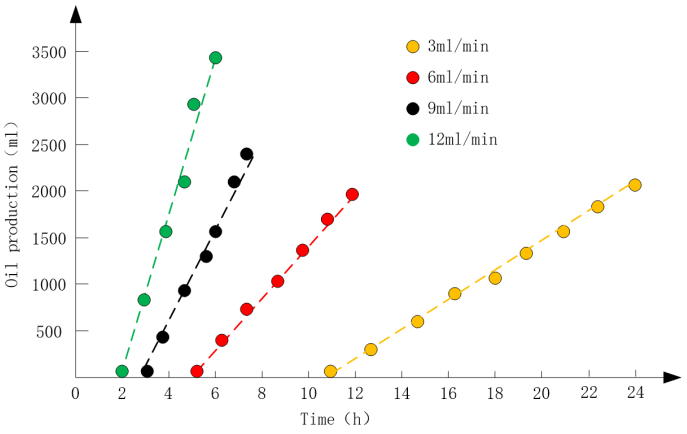

Figure 11. Law of change of water production with time.

The fitting functions of total production volume with time under different water injection rates are as follows:

- Injection rate of 3 ml/min:

$$y = 148.08x - 1555.8, \quad R^2 = 0.9956$$

- Injection rate of 6 ml/min:

$$y = 303.22x - 1489.7, \quad R^2 = 0.9968$$

- Injection rate of 9 ml/min:

$$y = 529.54x - 1669.6, \quad R^2 = 0.9942$$

- Injection rate of 12 ml/min:

$$y = 913.88x - 1979.3, \quad R^2 = 0.9855$$

These results are shown in Figure 12.

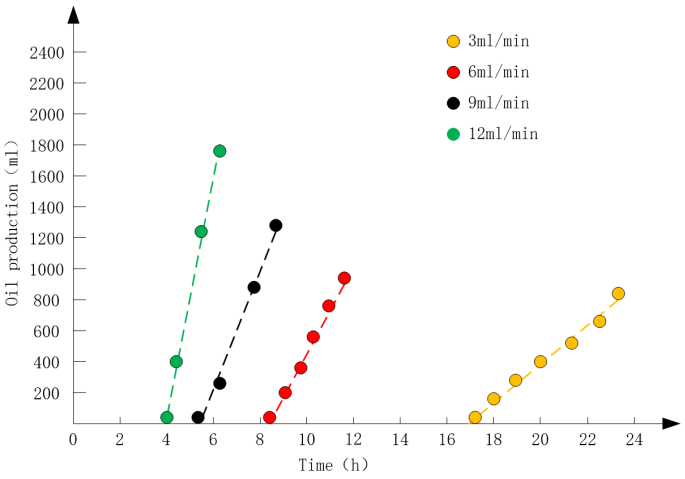

Figure 12. Liquid production with time change rule.

As can be seen from Figures 10–12, the oil production increases logarithmically with the water injection time, while the water and liquid production increase linearly. When the injection rate is 12 ml/min, the oil, water and liquid production increase the fastest, and at 3 ml/min, the increase is the smallest. That is to say, with the increase of the injection rate, the oil, water and liquid production increase faster. The 3 ml/min injection rate exhibits a significant difference in time and acceleration compared with other rates, indicating that the kinetic energy at 3 ml/min is too small to effectively drive the transport of crude oil.

It is further calculated that the oil production, water production and liquid production vary with the injection volume multiplier (PV) under different injection rates. The fitting functions for oil production as a function of PV are as follows:

- Injection rate of 3 ml/min:

$$y = -4819.8x^2 + 9747.6x - 3838.3, \quad R^2 = 0.9992$$

- Injection rate of 6 ml/min:

$$y = -4138.6x^2 + 8493.9x - 3178.2, \quad R^2 = 0.9965$$

- Injection rate of 9 ml/min:

$$y = -3149.4x^2 + 7105.8x - 2551.4, \quad R^2 = 0.9851$$

- Injection rate of 12 ml/min:

$$y = -3795.8x^2 + 8109.9x - 2611.9, \quad R^2 = 0.9939$$

These results are shown in Figure 13.

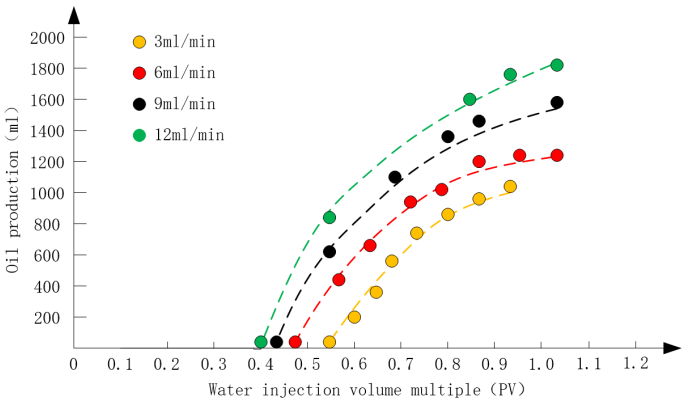

Figure 13. Change pattern of oil production with PV.

The fitting functions for water production as a function of PV under different water injection rates are as follows:

- Injection rate of 3 ml/min:

$$y = 2657.5x - 2218.6, \quad R^2 = 0.9967$$

- Injection rate of 6 ml/min:

$$y = 2934.3x - 2426.2, \quad R^2 = 0.9993$$

- Injection rate of 9 ml/min:

$$y = 3674.8x - 3041.7, \quad R^2 = 0.9999$$

- Injection rate of 12 ml/min:

$$y = 5040.4x - 3948.3, \quad R^2 = 0.9891$$

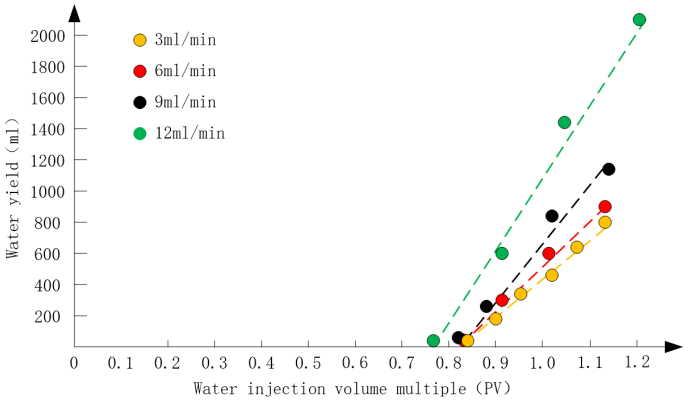

Figure 14. Changing law of water production with PV.

These results are shown in Figure 14.

The fitting functions for liquid production as a function of PV under different water injection rates are as follows:

- Injection rate of 3 ml/min:

$$y = 3043.8x - 1555.8, \quad R^2 = 0.9956$$

- Injection rate of 6 ml/min:

$$y = 3116.5x - 1489.7, \quad R^2 = 0.9968$$

- Injection rate of 9 ml/min:

$$y = 3628.3x - 1669.6, \quad R^2 = 0.9942$$

- Injection rate of 12 ml/min:

$$y = 4696.3x - 1978.3, \quad R^2 = 0.9855$$

These results are shown in Figure 15.

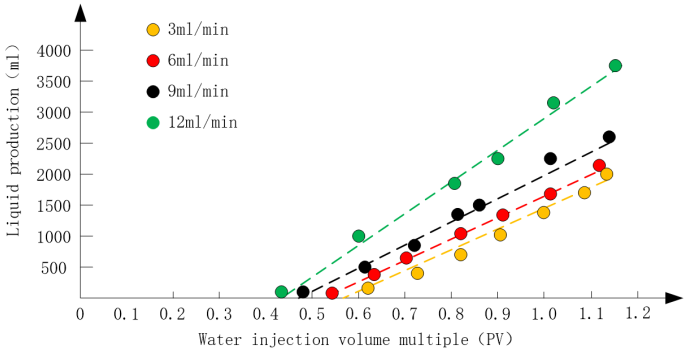

Figure 15. Change rule of liquid production with PV.

As can be seen through Figures 13–15, the change rule of oil production, water production and liquid production is the same as that of time, and the oil production is gradually levelling off. Water production, liquid production increases with the increase of injection volume times, and the larger the injection rate, the more obvious the increase in production. It can be seen that the starting point of each data are different between 0.1PV, but 12ml/min will be other parameters under the oil production time pulled relatively large gap.

According to the above experiments, the best recovery effect can be obtained when the water injection rate reaches 12ml/min and the injection volume multiplier reaches 1.0-1.1. The study area belongs to high steep and extremely complex fault block structure oil and gas reservoir. The fracture block type is subdivided into three types: open, semi-closed and closed. So according to the real working conditions, the experimental data were converted by similarity criterion, and the samples of well groups A (water wells in low part of the formation) and B (oil wells in high part of the formation), and C (water wells in high part of the formation) and D (oil wells in low part of the formation) in the mine site were selected as the preferred samples (Figure 16). The case study of water injection project was conducted for 8-12 months under two scenarios of low water injection and high oil recovery and high water injection and low oil recovery.

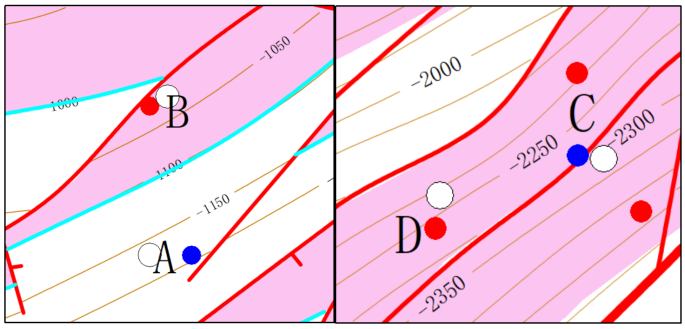

Figure 16. Tectonic diagram of low injection and high extraction (AB) and high injection and low extraction (CD) well groups.

It can be concluded from Table 1 that, in the low-injection and high-production well group in the field, the daily water injection rate of well A (located in the structurally low position) was gradually increased from 7.2 t/d to approximately 13 t/d. As a result, the daily oil production of well B (located in the structurally high position) increased gradually. When the injection rate of well A was further raised to about 24 t/d, the daily oil production of well B showed a rapid upward trend, indicating a clear and positive response to water injection.

It can be concluded from Table 2 that, in the high-injection and low-production well group on site, the daily injection rate of water well C (located in the structurally high position) was maintained at approximately 20 t/d. The corresponding oil well D showed a gradual decrease in daily liquid production, while the daily oil production first increased slightly and then stabilized. When the injection rate of well C was further increased to about 28 t/d, the daily liquid production of well D increased, but the daily oil production decreased, indicating an obvious water channeling phenomenon.

To sum up, with the increase of water injection rate in low injection and high recovery, the daily liquid and daily oil level gradually increase, and under the high water injection rate, the oil producing wells respond to injection obviously; high injection and low recovery wells group, the average injection rate of oil producing wells respond to injection is lower than the low injection and high recovery injection rate, with the further increase of water injection rate, the wells see the increase of daily liquid level, and the decrease of daily oil level, and there is obvious water flushing phenomenon. It shows that the inclination angle of the formation has an effect on the water injection rate and oil recovery efficiency: high injection and low recovery wells group relative to low injection and high recovery wells group, affected by gravity, the power provided by the water injection rate is more likely to overcome the reservoir pore throat capillary force, friction and other resistance, which corresponds to the wells are more likely to see oil. Therefore, for the high injection and low recovery well group, the water injection rate is smaller than the low injection and high recovery well group, and beware of the phenomenon of water channeling.

5 Discussion

5.1 Physical Mechanisms Underlying the Observed Injection-Rate Effects

The experimental results collectively demonstrate that water injection rate is a governing parameter controlling both the displacement dynamics and residual oil distribution in the Tankou oilfield fault-block reservoir. The acceleration of oil and water breakthrough times with increasing injection rate is consistent with the capillary-number framework: higher flow velocities increase the ratio of viscous forces to capillary forces, mobilising oil that would otherwise remain trapped by interfacial tension [3]. This observation aligns with the findings of Arab et al. [19], who established that injection velocity is a primary determinant of the oil–water force balance during waterflooding, and with Chen et al. [4], who demonstrated analogous rate-dependent fluid mobilisation in tight-oil cores using NMR.

The logarithmic decline of residual oil saturation with increasing injection rate reflects a pore-scale mechanism: as injection velocity rises, viscous pressure overcomes capillary resistance in progressively smaller pore throats, accessing oil that is inaccessible at lower rates. This relationship has a physical upper limit, evidenced by the binomial inflection in the recovery–rate curve at approximately 15 ml/min. Beyond this threshold, further rate increases yield diminishing returns because the capillary pressure in the finest pore throats cannot be overcome under the prevailing conditions, consistent

Table 1. Comparison of preferred wells for low injection and high recovery.

Times	Water well (A)	Oil well (B)			
	Daily injection level (t)	Daily fluid level (t)	Daily oil level (t)	Containing water (%)	Dynamic fluid level (m)
2023.3	0	0.9	0.8	11.11	509.5
2023.4	7.2	1.2	1.0	16.67	1013
2023.5	13.3	1.2	1.2	0.00	1018
2023.6	26.1	1.4	1.4	0.00	503.5
2023.7	22.5	1.9	1.9	0.00	501.5
2023.8	23.1	2.4	2.4	0.00	512
2023.9	22.7	2.7	2.5	7.41	512
2023.10	24.2	3.2	2.8	12.50	509
2023.11	24.2	3.0	2.9	3.33	518
average	18.14	1.99	1.88	5.67	–
total	163.3	17.9	16.9	–	–

Table 2. Comparison of preferred wells for high injection and low extraction.

Times	Water well (C)	Oil well(D)			
	Daily injection level(t)	Daily fluid level(t)	Daily oil levels(t)	Containing water(%)	Dynamic fluid level(m)
2022.12	-	10.1	9.4	6.93	1091.5
2023.1	19.6	10.1	9.5	5.94	1091.5
2023.2	22.5	9.8	9.1	7.14	2183
2023.3	20.1	9.7	9.2	5.15	2183
2023.4	19.5	8	7.6	5.00	2183
2023.5	20	8.4	8	4.76	2183
2023.6	20.3	8.3	7.9	4.82	2183
2023.7	21.5	7.8	7.4	5.13	2183
2023.8	26.4	6.5	6.1	6.15	2183
2023.9	15.8	6.4	6.1	4.69	2183
2023.10	16.4	6.1	4.9	19.67	2183
2023.11	25.8	6.9	6.1	11.59	2193
2023.12	28.5	7.2	6.2	13.89	2193
average	18.3	8.3	7.7	7.76	-
total	256.4	116.6	107.6	7.72	-

with the pore-throat-radius-dependent displacement limit reported in the literature [13]. The linear growth of water and liquid production with pore-volume multiplier, combined with the logarithmic growth of oil production with time, reflects the progressive exhaustion of readily mobilisable oil and the onset of water channeling along high-permeability pathways, as described by Jiang et al. [16] and Wang et al. [17].

The disproportionately poor performance at 3 ml/min—characterised by significantly longer production timescales and lower acceleration compared with the other rates—indicates that this rate falls below the minimum threshold required to generate sufficient viscous force for effective crude oil transport across the model. This threshold behaviour is consistent with the concept of a critical capillary number below which displacement efficiency deteriorates sharply.

5.2 Influence of Formation Dip on Optimal Injection Rate

A key engineering finding of this study is that the optimal injection rate differs systematically between low-injection–high-production (LI-HP) and high-injection–low-production (HI-LP) well configurations, and that this difference is attributable to the high-angle dip structure (45°–60°) characteristic of the Tankou oilfield. In the LI-HP configuration (water well in the structurally low position, oil well in the structurally high position), the injected water must overcome both capillary resistance and the gravitational component opposing upward migration, necessitating a higher injection rate to generate sufficient kinetic energy. In contrast, in the HI-LP configuration (water well in the structurally high position, oil well in the structurally low position), gravity acts in the direction of displacement, reducing the injection rate required to initiate effective oil transport. However, this gravity-assisted driving force also increases the risk of water channeling: at excessive injection rates, water preferentially advances along high-permeability pathways to the production well, creating an unbalanced sweep and leaving substantial residual oil in bypassed zones [15, 16]. These dip-dependent effects highlight that injection-rate optimisation cannot be divorced from structural geology, a consideration that is often insufficiently emphasised in injection-rate studies conducted on horizontal or low-dip models [6, 14].

5.3 Comparison with Previous Studies and Novelty of This Work

Previous studies on injection-rate effects in water-driven oil systems have predominantly relied on either pore-scale numerical simulation or single-dimensional core-flooding experiments, with relatively few incorporating three-dimensional physical models validated against field data [1, 2]. Sun et al. [12] identified the limitation that commercial reservoir simulators cannot capture the dynamic variation of residual oil saturation

with water drive velocity, and proposed a corrected numerical framework; the present study provides complementary physical-experimental evidence that supports the existence of this rate-dependent saturation relationship. Wang et al. [17] demonstrated that the waterflooding front in heterogeneous low-permeability reservoirs advances non-uniformly with injection rate, consistent with the diagonal arc displacement trajectory observed in this study's flow-trace visualisation. The present work extends these findings by simultaneously quantifying the plane and longitudinal residual oil distribution under four injection rates in a three-dimensional model representative of a specific fault-block reservoir, and by linking the laboratory results to field implementation through similarity-criterion conversion.

The integrated methodology—combining three-dimensional physical modelling, resistance-based oil-saturation mapping, flow-trace visualisation, and field data verification—represents an advance over studies that rely on a single experimental or simulation approach [13]. The mathematical empirical models established here (logarithmic for oil production vs. time, linear for water and liquid production vs. time, binomial for recovery degree vs. injection rate, and logarithmic for residual oil saturation vs. injection rate) provide a practical quantitative framework that can be directly translated to field injection parameters via similarity criteria.

5.4 Limitations and Future Work

Several limitations constrain the generalisability of the present findings. First, the experiments were conducted exclusively with 200-mesh quartz sand, which represents a single, homogeneous pore-size distribution; real reservoir heterogeneity—including interlayer permeability variation, clay content, and fracture presence—was not simulated. Second, all experiments were performed at horizontal inclination and atmospheric pressure; the combined effects of formation dip, overburden pressure, and reservoir temperature on the optimum injection rate remain to be quantified. Third, the three sample pairs used for field validation (well groups A–B and C–D) may not be fully representative of the entire X well area given the high structural complexity and block-to-block variability of the Tankou oilfield. Future work should address these limitations through: (i) experiments with variable grain-size distributions and layered heterogeneous models; (ii) high-pressure, elevated-temperature simulation to replicate actual downhole conditions; and (iii) expanded field data collection across a larger number of well groups to statistically validate the similarity-criterion conversions.

6 Conclusion

It can be determined through experimental demonstration that the higher the injection rate, the higher the recovery rate, but there is an upper limit. When the injection rate reaches the upper limit, it can not overcome the capillary force under the small pore throat radius, so under the real working condition, the water injection development can only drive off the remaining oil under a certain pore throat radius. At the same time we also found:

(1) The 3 ml/min water injection rate shows a significantly larger difference in time and acceleration compared with the other rates, indicating that the kinetic energy of 3ml/min injection rate is too small, difficult to drive the transport of crude oil; when the injection rate reaches 12ml/min, the shortest time to see water and oil, the fastest rate. The final recovery degree reaches 80%, the final residual oil saturation reaches 0.15, according to the mathematical formula for fitting the injection rate and the final recovery degree, the best injection rate of the experiment is expected to be 15ml/min, which indicates that the kinetic energy possessed by the injection rate of 15ml/min has reached the upper limit of the capillary resistance in the microscopic pore throats of the drive reservoir, and the recovery degree has reached the maximum value.

(2) low-injection high-production well group by gravity, the kinetic energy required to drive oil is greater than the high injection of low-production well group, the water injection rate is also greater than the high injection of low-production well group water injection rate.

(3) As a next step, the optimal injection rate derived from the experiment can be converted to the real injection volume on site through the similarity criterion, and in the case of low injection and high extraction, the daily injection of 24 m^3can be implemented; in the case of high injection and low extraction, the daily injection of 20 m^3 can be implemented to verify the effect.

Data Availability Statement

Data will be made available on request.

Funding

This work was supported without any funding.

Conflicts of Interest

Yuan Yang is affiliated with the Exploration and Development Research Institute, Jianghan Oilfield Company, Sinopec, Wuhan 430223, China. Ye Yang is affiliated with the Drilling Company No.1 of Sinopec Jianghan Petroleum Engineering Co., Ltd., Qianjiang, 433123, China. The authors declare that these affiliations had no influence on the study design, data collection, analysis, interpretation, or the decision to publish, and that no other competing interests exist.

AI Use Statement

The authors declare that no generative AI was used in the preparation of this manuscript.

Ethical Approval and Consent to Participate

Not applicable.

References

[1] Zhou, W., Yin, D., & Zhou, Y. (2023, September). The seepage mechanism of Micro remaining oil during Cyclic waterflooding in Low-permeability reservoir. In *Journal of Physics: Conference Series* (Vol. 2584, No. 1, p. 012021). IOP Publishing. [CrossRef]

[2] Yin, K. (2023). Present situation and development trend of oil production technology in unstable waterflooding. *Advances in Resources Research, 3*(1), 17-31. [CrossRef]

[3] Wang, Y., Han, X., Li, J., Liu, R., Wang, Q., Huang, C., ... & Lin, R. (2023). Review on oil displacement technologies of enhanced oil recovery: state-of-the-art and outlook. *Energy & Fuels, 37*(4), 2539-2568. [CrossRef]

[4] Chen, M., Dai, J., Liu, X., Kuang, Y., Wang, Z., Gou, S., ... & Li, M. (2020). Effect of displacement rates on fluid distributions and dynamics during water flooding in tight oil sandstone cores from nuclear magnetic resonance (NMR). *Journal of Petroleum Science and Engineering, 184*, 106588. [CrossRef]

[5] Tan, Y., Zhang, Y., Hui, C., Yu, C., Tian, S., Wang, T., & Wang, F. (2023). Resonance-enhanced pulsing water injection for improved oil recovery: Micromodel experiments and analysis. *Processes, 11*(3), 957. [CrossRef]

[6] Liu, G., Wang, H., Tang, J., Liu, Z., & Yang, D. (2023). Effect of wettability on oil and water distribution and production performance in a tight sandstone reservoir. *Fuel, 341*, 127680. [CrossRef]

[7] Saadat, M., Vikse, N. B., Øye, G., & Dudek, M. (2021). A microfluidic study of oil displacement in porous media at elevated temperature and pressure. *Scientific Reports, 11*(1), 20349. [CrossRef]

[8] Xu, J., Aghabarati, H., Zamani, A., & Zambrano, J. A. (2023, March). Utilizing Gas/Water Displacement in Oil Sands Reservoir for Lean Zone Mitigation. In *SPE Canadian Energy Technology Conference* (p. D021S013R003). SPE. [CrossRef]

[9] Zhang, Y., Li, B., Lu, T., Li, Z., Zeng, X., & Song, Y. (2023). Adaptation study on nitrogen foam flooding in thick reservoirs with high water cut and high permeability. *Colloids and Surfaces A: Physicochemical and Engineering Aspects, 657*, 130539. [CrossRef]

[10] Shapoval, A., Zhuravljov, A., Lanetc, Z., & Rahman, S. S. (2023). Pore-scale evaluation of physicochemical interactions by engineered water injections. *Transport in Porous Media, 148*(3), 605-625. [CrossRef]

[11] Wei, J., Zhou, X., Shi, X., Gong, P., Chen, Y., Wang, Y., ... & Zhou, R. (2023). Remaining oil distribution and recovery performances with waterflooding and surfactant-polymer flooding: An experimental investigation. *International Journal of Hydrogen Energy, 48*(23), 8430-8439. [CrossRef]

[12] Sun, Z., Liu, Y., Cai, H., Gao, Y., & Jiang, R. (2023). The numerical simulation study on the dynamic variation of residual oil with water drive velocity in water flooding reservoir. *Frontiers in Energy Research, 10*, 977109. [CrossRef]

[13] Xiao, L., Zhu, G., Zhang, L., Yao, J., & Sun, H. (2021). Effects of pore-size disorder and wettability on forced imbibition in porous media. *Journal of Petroleum Science and Engineering, 201*, 108485. [CrossRef]

[14] Wang, L., He, Y., Chen, H., Meng, Z., & Wang, Z. (2019). Experimental investigation of the live oil-water relative permeability and displacement efficiency on Kingfisher waxy oil reservoir. *Journal of Petroleum Science and Engineering, 178*, 1029-1043. [CrossRef]

[15] Cao, B., Xie, K., Lu, X., Cao, W., He, X., Xiao, Z., ... & Su, C. (2021). Effect and mechanism of combined operation of profile modification and water shutoff with in-depth displacement in high-heterogeneity oil reservoirs. *Colloids and Surfaces A: Physicochemical and Engineering Aspects, 631*, 127673. [CrossRef]

[16] Jiang, Z., Ren, H., Maimaitiming, D., Wang, Z., & Dong, H. (2023). Effects of water flooding speed on oil recovery efficiency and residual oil distribution in heterogeneous reservoirs. *Petroleum Science and Technology, 41*(24), 2362-2375. [CrossRef]

[17] Wang, C., Sun, Z., Sun, Q., Zhang, L., & Zhang, X. (2021). Comprehensive evaluation of waterflooding front in low-permeability reservoir. *Energy Science & Engineering, 9*(9), 1394-1408. [CrossRef]

[18] Chen, T., Yang, Z., Luo, Y., Lin, W., Xu, J., Ding, Y., & Niu, J. (2018). Evaluation of displacement effects of different injection media in tight oil sandstone by

online nuclear magnetic resonance. *Energies*, *11*(10), 2836. [CrossRef]

[19] Arab, D., Kantzas, A., & Bryant, S. L. (2020). Water flooding of oil reservoirs: Effect of oil viscosity and injection velocity on the interplay between capillary and viscous forces. *Journal of Petroleum Science and Engineering*, *186*, 106691. [CrossRef]

[20] Li, Y., Liu, D., Zhao, L., Wang, R., Xu, H., Liu, L., ... & Si, Y. (2024). Research on flow field reconstruction of complex fault-block reservoir during ultra-high water cut period. *Discover Applied Sciences*, *7*(1), 39. [CrossRef]

[21] Liu, Y., Luo, J., Li, M., Guo, L., Yuan, J., & Zhang, L. (2017). Structural model and exploration potential in Tankou block of Qianjiang sag, Jianghan Basin. *China Petroleum Exploration*, *22*(4), 84-89. [CrossRef]

[22] Lu, H., Shen, C., Zhang, Z., Liu, M., Sheng, G., Peng, P. A., & Hsu, C. S. (2015). 2, 3, 6-/2, 3, 4-aryl isoprenoids in Paleocene crude oils from Chinese Jianghan Basin: Constrained by water column stratification. *Energy & Fuels*, *29*(8), 4690-4700. [CrossRef]

[23] Xu, H., Wang, L., Cao, Y., Yu, T., Tang, H., & Lin, J. (2022). Experimental research of remaining oil distribution for inverted nine-sport pattern and infill well pattern. *Arabian Journal for Science and Engineering*, *47*(9), 11297-11312. [CrossRef]

[24] Li, Q. (2021, February). Description and Understanding of Complex Fault Block Reservoir Geology. In *IOP Conference Series: Earth and Environmental Science* (Vol. 651, No. 3, p. 032033). IOP Publishing. [CrossRef]

[25] Wang, H., Yin, T., & Wang, S. (2017). Stratigraphic correlation and division of the salite strata. *Acta Geologica Sinica-English Edition*, *91*(s1), 138-139. [CrossRef]

[26] Li, J. (2018, November). Key technology and application of multilevel complex fault block reservoir description. In *AIP Conference Proceedings* (Vol. 2036, No. 1, p. 030049). AIP Publishing LLC. [CrossRef]

[27] Cui, C., Li, J., Wu, Z., Zong, R., Kong, W., Li, L., ... & Su, S. (2023). Simulation analysis of the mechanism and influencing factors of remaining oil secondary enrichment in ultra-high water cut fault block reservoirs. *Energy Exploration & Exploitation*, *41*(4), 1189-1208. [CrossRef]

Yuan Yang Received the Ph.D. degree from Yangtze University, Wuhan, Hubei, China, in 2022. (Email: fengjiming@yeah.net)

Ye Yang Received the Ph.D. degree in Energy Science and Engineering from the School of Energy Science and Engineering, Central South University, Changsha 410083, China, in 2024. (Email: Kalimoto1977@yeah.net)